Journal of Molecular Liquids 377 (2023) 121518

Contents lists available at ScienceDirect

Journal of Molecular Liquids

journal homepage: www.elsevier.com/locate/molliq

Computer simulation study of ion-water and water-water hydrogen bonds in methanesulfonic acid solutions at room temperature

Manel Canales *, Elvira Guàrdia

Departament de Física, Universitat Politècnica de Catalunya, Campus Nord-Edifici B4-B5, Jordi Girona 1-3, Barcelona E-08034, Spain

ARTICLE INFO

Article history:
Received 14 November 2022
Revised 10 February 2023
Accepted 19 February 2023
Available online 23 February 2023

Keywords:
Aqueous methanesulfonic acid solutions
Molecular dynamics simulations
Viscosity and diffusion
Structural properties
Hydrogen bond networks
Continuous and interrupted hydrogen bond lifetimes

ABSTRACT

Classical molecular dynamics simulations of aqueous methanesulfonic acid solutions have been conducted at room temperature in the entire composition range. The dissociation of the acid has been considered according to the available experimental data. Then, the systems are constituted by the following molecular species: water and methanesulfonic acid molecules, hydronium cations, and mesylate anions. The simulations have been carried out employing a reliable force field, which provides density values that show an excellent agreement with the available experimental data. The shear viscosity, the diffusion coefficients of the molecular species, and the radial distribution functions, which involve water molecules, have also been computed. We have observed that water molecules diffuse faster than the other species at all concentrations. Moreover, the shear viscosity and the diffusion coefficients exhibit a noticeable unimodal concentration dependence with extrema located at 90 wt% (0.628 mol fraction). A detailed hydrogen bond analysis, concerning water molecules, has also been made. At low dilutions, water exhibits its well-known hydrogen bond tetrahedral structure, which vanishes as the acid concentration increases. The most labile water molecules are those bonded to the anions. At large concentrations, the lability of the water molecules, bonded to other water molecules, increases, and that of the water molecules, bonded to the cations, decreases. The interrupted lifetimes also show a unimodal dependence with maxima located at 90 wt%. This behavior could be related to the appearance of the methanesulfonic acid hydrogen bond network, which emerges at large weight percentage values because the acid almost completely dissociates up to concentrations of 70 wt% (0.304 mole fraction).

1. Introduction

Methanesulfonic acid (CH_3SO_3H, MSA) is the most common and simplest of the alkyl sulfonic acids [1]. At room temperature is a hygroscopic odorless, colorless, and low volatile liquid (vapor pressure: 1 mmHg at 20 °C) with a high boiling point (122 °C at 1 mmHg) [2]. MSA is a strong acid [3] ($pK_a = -1.9$), which completely ionizes in water at 0.1 M concentrations. In addition, it has moderate corrosivity and high conductivity, and its metal salts are soluble in water. In some applications, it is employed instead of sulfuric acid (SA) because MSA is a non-oxidizing agent, and it shows good thermal stability. In addition, it is less corrosive and toxic than SA and other chemicals, such as fluoroboric or fluorosilicic acids. Then, its storage, transport, and handling are much easier. Finally, it is an easily biodegradable substance, ultimately forming sulfate and carbon dioxide, and facilitating effluent treatment. MSA is widely employed in the industry. Then, it is normally used as an electrolyte in many electrochemical processes, especially those involving tin and lead. Moreover, it is also utilized to increase the conductivity of several polymers [4], as a catalyst in esterification and alkylation processes, and the leaching of metals [5].

It is well-known that aerosols affect the air Earth's albedo and climate. Indeed, aerosols in the atmosphere influence its physical and chemical properties because, on one hand, they scatter and absorb solar radiation, and on the other hand, they act as cloud condensation and ice nuclei, which affect the formation and evolution of clouds [6]. One of the most important aerosol sources is dimethyl sulfide ($(CH_3)_2S$, DMS), which is mainly generated in the oceans by marine phytoplankton, according to the global sulfur cycle [7]. DMS oxidizes and forms some sulfur compounds, such as SA and MSA [8,9]. Moreover, aqueous SA and MSA aerosols, which are binary mixtures of these acids and water, are also present in the stratospheric aerosol layer.

The study of aqueous MSA solutions is a very interesting topic because these systems are the electrolyte of choice in many electrochemical processes. Moreover, it can be assumed that aqueous MSA aerosols are concentrated aqueous MSA solutions. Experi-

* Corresponding author.
E-mail address: manel.canales@upc.edu (M. Canales).

https://doi.org/10.1016/j.molliq.2023.121518
0167-7322/

mental measurements of the density [10] of aqueous MSA solutions at 20, 25 and 35 °C, and the complex index of refraction and the surface tension [11], in a wide range of concentrations, have been published. Moreover, classical Molecular Dynamics (MD) simulation studies of pure MSA have been recently reported [12,13]. However, to our knowledge there are not any computer simulation works on aqueous MSA solutions, and only a scarce number of theoretical studies on this topic can be found in the literature. Then, Krishtal *et al.* [14] employed Density Functional Theory (DFT) methods to analyze the influence of the structure on the polarizability of hydrated MSA clusters. Wang [15] and Li *et al.* [16] analyzed the structures, molecular energies, and ionic dissociation of MSA hydrated clusters also using *ab-initio* methodologies. Finally, Kreidenweis and Seinfeld [17] applied the binary nucleation theory to study the formation of aqueous MSA aerosol particles in humid atmospheres.

MSA is a relatively strong hygroscopic acid that dissociates in water according to the following reaction:

$$CH_3SO_3H + H_2O \rightleftarrows CH_3SO_3^- + H_3O^+$$

Bascombe and Bell [18], Covington *et al.* [19,20] and Clarke and Woodward [21] carried out several spectroscopic experiments to analyze the dependence of the dissociation constant α with the acid concentration. Later, Lund Myhre *et al.* [11] analyzed those results and suggested that at room temperature α varies with the acid weight fraction w, according to the following simple polynomial equation: $\alpha(w) = 1 - 0.3867w^2 - 0.6714w^4$, which is valid in the range $0 < w < 0.9$. Therefore, the constituent molecular species in an aqueous MSA solution are: H_2O, hydronium cations H_3O^+, methanesulfonate (or mesylate) anions $CH_3SO_3^-$, and MSA molecules CH_3SO_3H.

Hydrogen bonds (HB) are omnipresent in chemistry and biology [22,23]. Simulations of hydrogen-bonded liquids [24], such as water and aqueous solutions, allow us to get detailed information about these systems from a microscopic point of view. For instance, it is well-known that water exhibits a topologically complex HB three-dimensional tetrahedral network [25]. Moreover, Canales and Guàrdia [26,27] have recently carried out MD simulations of dilute and moderate aqueous SA solutions at several temperatures. They compute structural and dynamic properties, and they also conducted a HB analysis involving water molecules.

In the present work, we run a set of MD simulations of aqueous MSA solutions at room temperature in the entire composition range. First, we will look for a reliable force field. Later, we will compute structural, dynamical, and collective properties, such as the density, viscosity, and diffusion coefficients. The suitability of the force field will be checked by comparing some of these properties with the available experimental data. Finally, we will carry out a HB analysis that involves water molecules. In each case, the radial distribution functions, the mean number of HB, the percentages of molecular species, hydrogen bonded with a given number of water molecules, and the interrupted and non-interrupted lifetimes will be computed. The paper is organized as follows: the simulation details and the force field will be introduced in the following section. The results of the density, viscosity, radial distribution functions, and HB analyses will be detailed in Section III. Finally, the conclusions will be summarized in the last section.

2. Methodology

2.1. Force field

According to the dissociation process set out in the preceding section, simulations have been carried out considering the following molecular entities: water molecules (H_2O), hydronium cations (H_3O^+), MSA molecules (CH_3SO_3H), and mesylate anions ($CH_3SO_3^-$), which are plotted in Fig. 1. It is important to note that no stretching interactions have been assumed. Therefore, the intramolecular force field only has bending and torsional terms. The first one has been computed using the well-known functional form $V_{bend}(\theta) = \frac{1}{2}k_\theta(\theta - \theta_{eq})^2$, k_θ and θ_{eq} being, respectively, the force constant and the equilibrium bending angle. The equilibrium bond lengths, bending bond angles, and force constants are gathered in Table 1 and Table 2. For CH_3SO_3H and $CH_3SO_3^-$ we have employed the values published in our previous work on pure MSA [13]. In the special case of the $CH_3SO_3^-$ anion, we have used the S-O distance proposed by Arstila *et al.* [28] in their *ab initio* density functional study of sulfuric acid hydrates. For water, we have used the SPCE model [29]. This is a rigid three-site force field which performs quite well under ambient conditions, as has been shown by Vega and Abascal [30] and Pathirannahalage *et al.* [31] in their comprehensive studies of several water models. In fact, Vega and Abascal [30] stated that only another non-polarizable model, the TIP4P/2005 potential [32], would be better than the SPCE in some aspects. In addition, they also pointed out that polarization effects should be included, in order to have better potentials. One of the most promising advances in this direction is the series of BK models proposed by Kiss and Baranyai [33–38]. Nevertheless, the good results we obtained in our earlier studies of aqueous SA solutions [26,27] employing the SPCE force field, have encouraged us to carry out the present study using the same water model. For hydronium ions, we have employed the equilibrium bond length and bending angle values proposed by Kusaka *et al.* [39] in their computer simulation study of the sulfuric acid-water binary nucleation process. The bending k_θ force constant parameter was the one suggested by Telemann *et al.* [40] in their well-known flexible water model. The following dihedrals have been taken into account to compute the torsional term: H-C-S-O and H-O-S-O,C. Both show three minima,

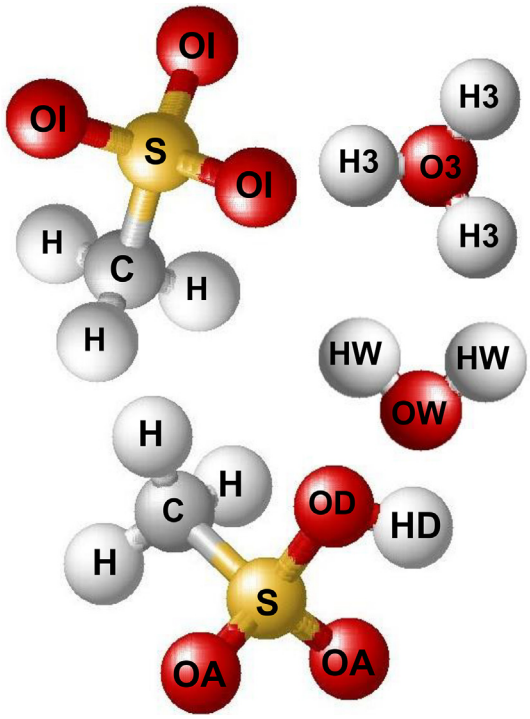

Fig. 1. Most favorable structures of the water and MSA (CH_3SO_3H) molecules, the hydronium H_3O^+ cations and the $CH_3SO_3^-$ anions. Labels correspond to the atom types defined in Tables 1-2 and Tables S1-S3 of the supplementary material.

Table 1
Equilibrium bond lengths (nm).

Bond	CH_3SO_3H	$CH_3SO_3^-$	H_3O^+	H_2O
C-H	0.1086[a]	0.1086[a]		
S-C	0.1788[a]	0.1788[a]		
S-OA,OI	0.1446[a]	0.1490[b]	–	–
S-OD	0.1631[a]	–	–	–
OD-HD,O3-H3,OW-HW	0.0968[a]	–	0.0973[c]	0.1000[d]

[a] Reference [13].
[b] Reference [28].
[c] Reference [39].
[d] Reference [29].

Table 2
Equilibrium bond angles θ_{eq} (degrees) and harmonic force constants $k\theta$ (kJmol^{-1}rad^{-2}).

	CH_3SO_3H		$CH_3SO_3^-$		H_3O^+		H_2O
Bond	θ_{eq}	k_θ	θ_{eq}	k_θ	θ_{eq}	k_θ	θ_{eq}
H-C–H	111.1[a]	276[a]	111.1[a]	276[a]			
H-C-S	107.8[a]	292[a]	107.8[a]	292[a]			
C-S-OD	100.6[a]	440[a]	–	–			
C-S-OA,OI	109.3[a]	440[a]	109.3[a]	440[a]	–	–	
OA-S-OD	107.1[a]	400[a]	–	–	–	–	
OA-S-OA, OI-S-OI	121.4[a]	460[a]	107.1[a]	460[a]	–	–	
S-OD-HD	107.5[a]	370[a]	–	–	–	–	
H3-O3-H3, HW-OW-HW	–	–	–	–	111.6[b]	383[c]	109.47[d]

[a] Reference [13].
[b] Reference [39].
[c] Reference [40].
[d] Reference [29].

the first one at −60°, 180° and 60°, and the second at −120°, 0° and 120°. The torsional interactions have been calculated according to the Ryckaert and Bellemans potential [41]: $V_{dihe}(\varnothing) = \sum_{n=0}^{5} C_n \cos^n(\varnothing - \pi)$, C_n being the parameters of the torsional force field, which are collected in Table S1 of the supplementary material.

The van der Waals interactions have been computed using the Lennard-Jones 12-6 potential. The homoatomic force field parameters for the four species are displayed in Table S2 of the supplementary material. The ones of CH_3SO_3H and $CH_3SO_3^-$ are those previously employed in our works on pure MSA [13] and aqueous sulfuric acid solutions [26,27]. The parameters of water molecules and hydronium ions are the ones of the SPCE model [29]. The geometric Lennard-Jones combination mixing rules have been applied to calculate the heteroatomic pair parameters.

Now we turn to the computation of the electrostatic contribution. It is important to point out that non-polarizable force fields, such as OPLS-AA, use partial charges which have been obtained assuming that the ionic species present in an aqueous solution are in their gas phase. An easy way to introduce the polarizability of water was recently proposed by Leontyev and Stuchebrukhov [42–46], who suggested scaling the ionic charges using the following simple relation $q_{scaled} = q/\sqrt{\varepsilon_{el}}$, ε_{el} being the high-frequency dielectric constant of water. In their series of papers, these authors showed that their methodology was equivalent to immersing the ions (or the molecules) in a continuum medium with its corresponding relative permittivity. At the same time, Kann and Skinner [47] proposed to employ $\varepsilon_{el} = \varepsilon_0/\varepsilon_{sim}$, where ε_0 is the experimental value of the dielectric constant of water, and ε_{sim} is the one of the models used in the simulation. This methodology has been recently followed by Canales and Guàrdia [27] and Zeron *et al.* [48] to study some ionic solutions. In our case, we have employed the SPCE model. Therefore, the charges of the anions and cations are respectively −0.9 and 0.9, instead of −1.0 and 1.0. The set of partial charges adopted in this work has been displayed in Table S3 of the supplementary material.

2.2. Computer simulation details

NPT-MD simulations have been carried out using the GROMACS 2020 series software package [49] with a time step of 1 fs and the usual periodic boundary conditions. The SHAKE procedure [50] has been used to keep constant all bond lengths. The Berendsen weak coupling pressure and the temperature bath algorithms [51] have been employed to fit the pressure and the temperature to 1 atm and 298 K. To this end, the temperature and the pressure coupling time constant values have been, respectively, 0.1 and 1 ps. The van der Waals interactions have been truncated at 1.2 nm. The Ewald summation methodology [52] has been adopted to calculate the electrostatic interactions. To this end, the real space term has been truncated at 1.2 nm (the van der Waals distance cut-off) and the reciprocal space contribution has been computed using the Particle Mesh Ewald [53] interpolation procedure, employing an infinite grid of points, being the grid spacing 0.12 nm.

The following procedure has been implemented to get an equilibrated starting structure for each system: First, a microscopic configuration has been generated introducing the molecules in a cubic box at random. Next, an energy minimization method (10^4 steps or more), which uses a steepest descent algorithm [54], has been applied. Finally, NPT-MD runs (2×10^7 time steps) have been carried out. The production runs consist of long (15 ns) NPT-MD simulations. In some cases, the coordinates and velocities have been written every 10 steps.

Twelve systems, in the acid weight percentage range $0 < wt\% < 100$, have been studied. In each case, the dissociation constant values proposed by Lund Myhre *et al.* [11], have been

Table 3
Simulation details: Concentration (wt%, mole fraction × and molality m), dissociation constant α (Reference 11) and number of molecules of every constituent species.

wt%	x	m	α	CH_3SO_3H	$CH_3SO_3^-$	H_3O^+	H_2O
0	0	–	–	–	–	–	4000
10	0.020	1.166	0.996	0	83	83	3917
20	0.045	2.609	0.983	3	184	184	3816
30	0.074	4.441	0.960	13	308	308	3692
40	0.111	6.938	0.921	40	460	460	3540
50	0.158	10.435	0.861	105	647	647	3353
60	0.220	15.597	0.774	254	871	871	3129
70	0.304	24.257	0.649	614	1136	1136	2864
80	0.429	41.630	0.477	1569	1431	1431	2569
90	0.628	93.640	0.246	2544	830	830	1170
95	0.781	197.7164	0.104	1596	185	185	315
100	1	–	–	2000	–	–	–

employed. The number of molecules of all the molecular entities in terms of the weight percentage wt% and the mole fraction x is summarized in Table 3.

3. Results and discussion

3.1. Density and viscosity

The simulation density results are gathered in Table 4 and Fig. 2, together with the experimental values measured by Teng and Lenzi [10] at 25 °C in the entire composition range. An excellent agreement is observed between both sets of data, which exhibit a monotonically increase as the concentration rises.

The shear viscosity has been computed employing the following Green-Kubo relationship [55]:

$$\eta = \frac{V}{kT}\int_0^\infty \langle P_{\alpha\beta}(t_0)P_{\alpha\beta}(t+t_0)\rangle dt,$$

which relates this coefficient with the autocorrelation function of the off-diagonal components of the stress tensor $P_{\alpha\beta}(t)$. A careful analysis of the autocorrelation function tail is required to compute this quantity [56] To this end, simulations of up to 15 ns have been carried out. Moreover, the correlation functions have been analyzed up to 1 ns for concentrated solutions. The simulation data have also been displayed in Table 4 and Fig. 2. To our knowledge, there are no experimental data on the viscosity in terms of the concentration, but there are only results for pure water and MSA. In the first case, a notorious discrepancy between the simulation result of 0.71 cP and the experimental value of 0.896 cP has been observed, which Gonzalez and Abascal [56] also noticed. For pure MSA, a nice good agreement is observed between the experimental finding of 11.21 cP, reported by Roitman *et al.* [57] and the simulation result of 10.9 cP, gathered in Table 4. The shear viscosity exhibits a noticeable unimodal concentration dependence, with the maximum located at 90 wt% (x = 0.628). Rhodes and Barbour [58] reported a similar behavior for aqueous sulfuric acid solutions at concentrations close to 85 wt%, using experimental techniques. Isdale *et al.* [59] and Kay and Broadwater [60] also found the same unimodal dependence, but at lower concentrations, in their experimental studies of water-methanol and water-ethanol binary mixtures. Finally, Guevara-Carrion *et al.* [61] carried out MD simulations of the same systems, obtaining a nice good agreement with the experimental data.

Table 4
Simulation and experimental results of the density ρ (gcm^{-3}) (Reference 10) and viscosity η (cP) at room temperature.

wt%	ρ_{sim}	ρ_{exp}	η_{sim}
0	0.999	0.997	0.71
10	1.046	1.040	0.88
20	1.095	1.086	1.20
30	1.145	1.133	1.52
40	1.197	1.187	2.30
50	1.250	1.235	4.90
60	1.301	1.293	6.60
70	1.352	1.350	12.40
80	1.398	1.403	32.20
90	1.440	1.445	34.60
95	1.457	1.467	20.50
100	1.476	1.475	10.90

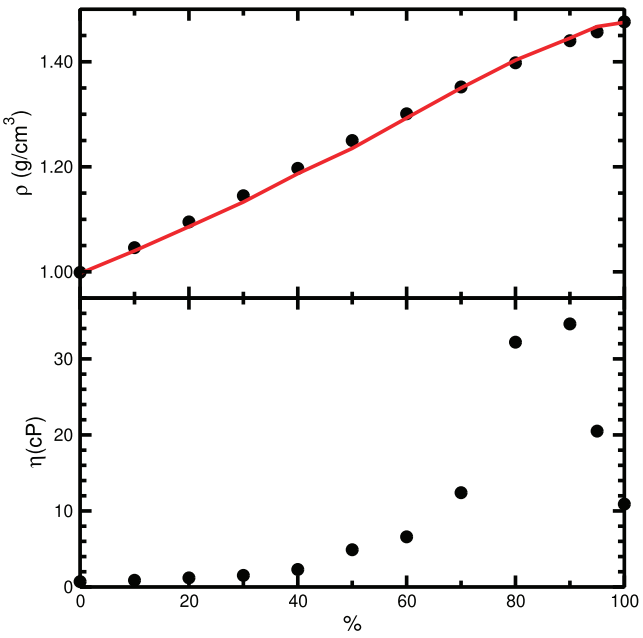

Fig. 2. Density and viscosity values in the whole concentration range at room temperature. Circles (simulation) and lines (experiment).

3.2. Self-diffusion coefficients

The self-diffusion coefficients of each molecular entity D_i have been calculated by analyzing the long-time behavior of the mean square displacements, using the Einstein equation [52]. The diffusion coefficients of the four species, in terms of the acid concentration, are depicted in a semi-log plot in Fig. 3 and gathered in Table S4 of the supplementary material. The diffusion coefficients decrease as the concentration rises, showing their minima for the concentration value at which the viscosity exhibits its maximum. Moreover, up to 80 wt% (x = 0.429), the diffusion coefficients of each molecular species verify the following relationship: $D_{H_2O} > D_{H_3O^+} > D_{CH_3SO_3^-} \approx D_{CH_3SO_3H}$. However, at higher concentra-

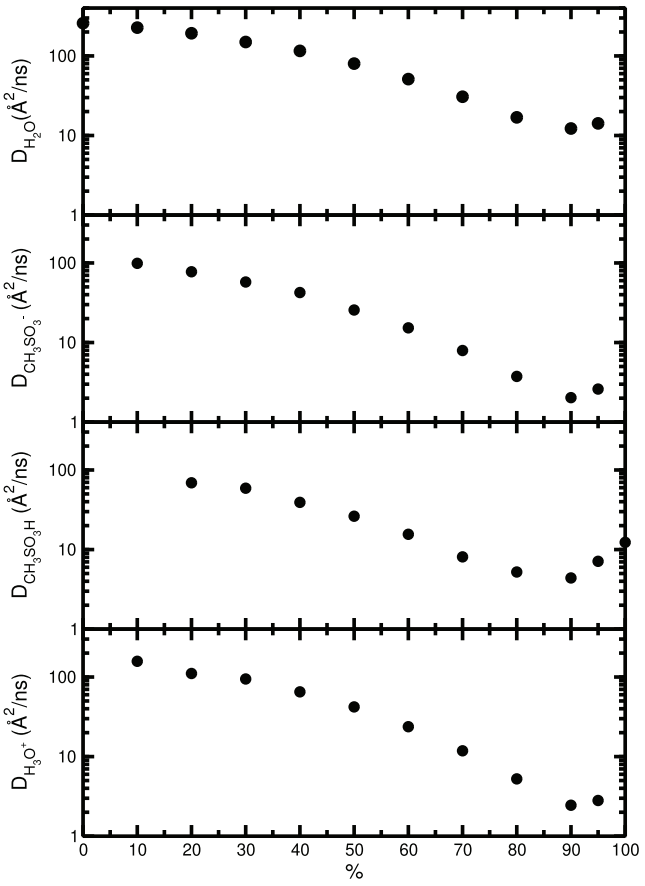

Fig. 3. Semi-log plot of the diffusion coefficients of water, $CH_3SO_3^-$ anions, MSA molecules and H_3O^+ cations, as a function of the concentration at room temperature.

tions, the relation is: $D_{H_2O} > D_{CH_3SO_3H} > D_{H_3O^+} \approx D_{CH_3SO_3^-}$. In any case, the water molecules are those that diffuse faster.

3.3. Analysis of hydrogen bonds

As we have stated in the introduction, we have performed a HB analysis involving water molecules. We have considered hydrogen bonds between hydrogen atoms of a given molecular specie, which are covalently bonded to oxygen atoms, and oxygen atoms with lone pairs of other molecular species. The oxygen atoms, which are bonded to the hydrogen ones, are named HB donors and the ones with lone pairs are named HB acceptors. Then, the oxygen atoms of the different molecular species considered in this study behave as follows: a) the oxygen atom of a hydronium ion is a HB donor, b) the oxygen atoms of a mesylate ion are HB acceptors, c) the oxygen atom of a water molecule can act as a HB acceptor or as a donor, d) the oxygen atoms of the sulfonyl group of each MSA molecule are HB acceptors; in this case the MSA molecule acts as an acceptor, which will be named MSA(acceptor). Finally, e) the oxygen atom of the hydroxyl group of each MSA molecule is a HB donor; in this case the MSA molecule acts as a donor that will be named MSA(donor). Therefore, the following HB can be considered: 1) those between water molecules, 2) the ones between water molecules and mesylate anions, 3) those between water and MSA(acceptor) molecules, 4) those between water molecules and hydronium cations, and 5) the ones between water and MSA(-donor) molecules. Fig. 4 and Fig. 5 will help us to understand the five types of HB. In Fig. 4 we have displayed the pictures of three characteristic configurations, with the oxygen atom of the water

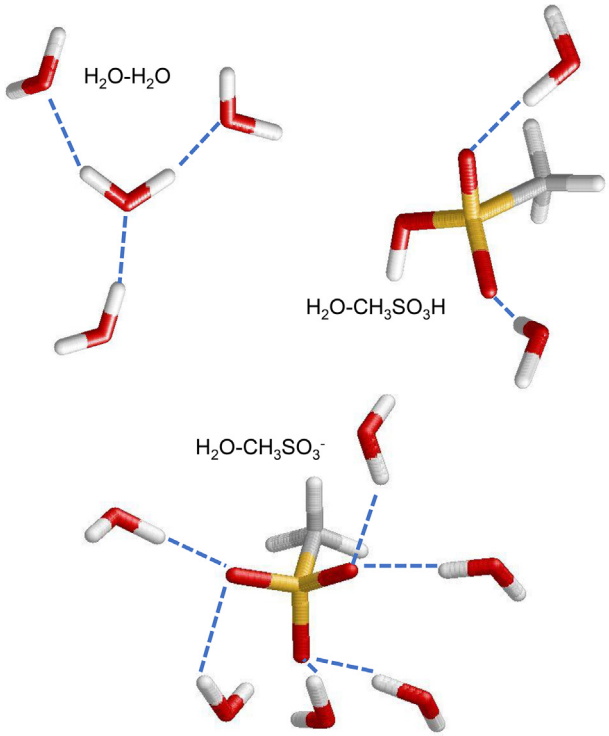

Fig. 4. Representative snapshots of the water-water, water-mesylate, and water-MSA(acceptor) hydrogen bonds at low dilutions.

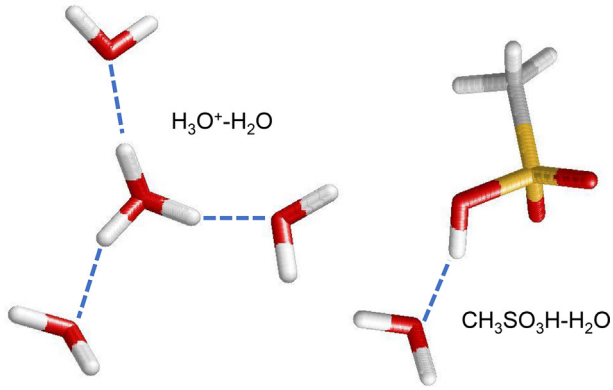

Fig. 5. Representative snapshots of the hydronium-water and MSA(donor)-water hydrogen bonds at low dilutions.

molecules OW behaving as a HB donor. The first one shows four water molecules interacting with each other. In this case, the oxygen atoms OW are both acceptors and donors. The second displays six water molecules interacting with one mesylate anion. In this situation, the water oxygens OW are donors and the mesylate oxygens OI are acceptors. In the third picture, two water molecules interact with one MSA molecule. Then, the oxygen atoms OA of the sulfonyl group of the MSA molecule are acceptors and the oxygen atom OW of every water molecule is a donor. In Fig. 5 we have plotted the pictures of two characteristic configurations with the oxygen atom of each water molecules OW acting as a HB acceptor. The first shows three water molecules interacting with one hydronium cation. In this case, the oxygen atom O3 of the hydronium ion is a donor, and each oxygen atom OW of a water molecule is an acceptor. The second picture shows one MSA molecule interacting with one water molecule. Then, the oxygen atom of the hydroxyl

group OD of the MSA molecule is a donor and the oxygen atom OW of the water molecule is an acceptor.

The HB analysis has been carried out employing the well-established geometric criterion [62,63], which states that two molecules are hydrogen bonded if the following three conditions are simultaneously accomplished: 1) the intermolecular oxygen-oxygen distance is smaller than the first minimum of the oxygen-oxygen radial distribution function, 2) the intermolecular hydrogen-oxygen separation is smaller than the first minimum of the hydrogen-oxygen radial distribution function and 3) the angle between the intermolecular oxygen-oxygen distance and the intermolecular oxygen-hydrogen bond is smaller than 30°.

3.4. Radial distribution functions

3.4.1. Water-water radial distribution functions

The $g_{OW\text{-}OW}(r)$ and $g_{OW\text{-}HW}(r)$ partial radial distribution functions at room temperature and concentrations of 20 wt%, 40 wt%, 60 wt %, 80 wt%, 90 wt% and 95 wt% (x = 0.045, 0.111, 0.220, 0.429, 0.628 and 0.781) are displayed in Fig. 6. At low dilutions both distribution functions are similar to those of pure water. Then, according to Mark and Nilsson [64], who carried out simulations of pure water employing the SPCE model, $g_{OW\text{-}OW}(r)$ exhibits three maxima located at 0.275, 0.45 and 0.685 nm, and two minima at 0.335 and 0.568 nm. Otherwise, $g_{OW\text{-}HW}(r)$ shows two maxima located at 0.177 and 0.325 nm, and one minimum at 0.241 nm. The concentration has a noticeable effect on the height of the $g_{OW\text{-}HW}(r)$ peaks, mainly at large values (80 wt%). Moreover, the concentration has a bigger incidence on $g_{OW\text{-}OW}(r)$. Indeed, the height of the first peak increases, the second and third peaks slightly shift to shorter distances and the first minimum becomes less apparent when the concentration rises. At moderate concentrations (40 wt%, x = 0.111) the minimum is almost imperceptible, and for more concentrated solutions the minimum and the second maximum merge giving rise to an appreciable slope, which indicates that the second water hydration layer vanishes. Then, it can be concluded that the averaged water structure is significantly modified by the presence of the acid. This finding is in qualitatively good agreement with the concluding remarks of Gallo *et al.* [65] in their MD study of potassium halide aqueous solutions at several concentrations. The partial structure factors $S_{OW\text{-}OW}(k)$ and $S_{OW\text{-}HW}(k)$, that could be useful to experimental X-ray and neutron diffraction researchers, have also been calculated and plotted in Fig. S1 of the supplementary material.

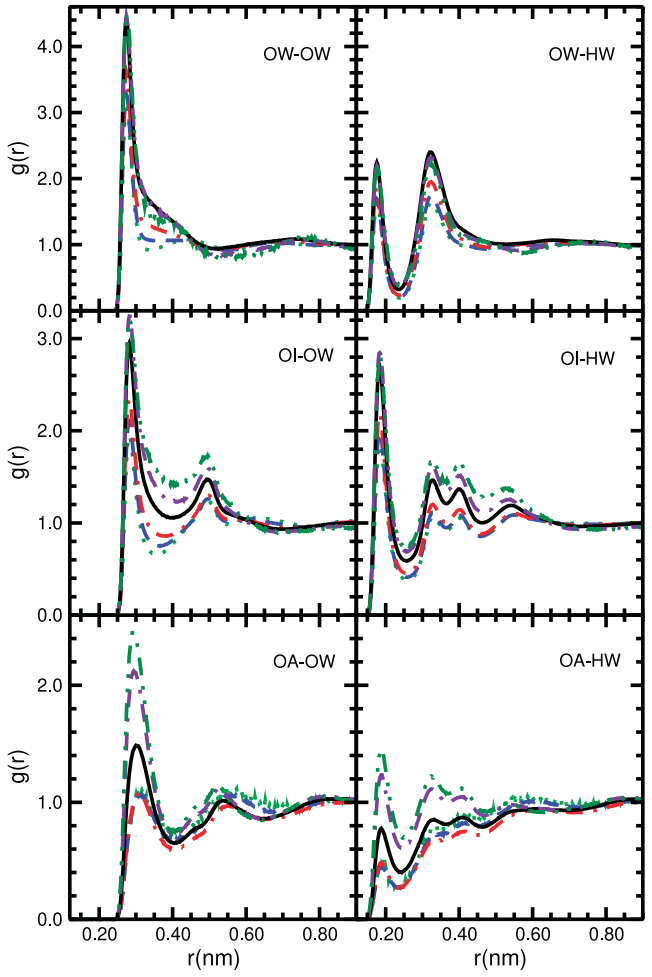

Fig. 6. Water-water, mesylate-water and water-MSA(acceptor) oxygen–oxygen and oxygen-hydrogen radial distribution functions at different concentrations: dotted line (green) 20 wt% (x = 0.045), dashed line (blue) 40 wt% (x = 0.111), dotted-dashed line (red) 60 wt% (x = 0.220), full line (black) 80 wt% (x = 0.429), dash-dash-dotted line (indigo) 90 wt% (x = 0.628) and dot-dot-dashed line (dark green) 95 wt% (x = 0.781). (For interpretation of the references to colour in this figure legend, the reader is referred to the web version of this article.)

3.4.2. Mesylate anion-water radial distribution functions

The $g_{OI\text{-}OW}(r)$ and $g_{OI\text{-}HW}(r)$ partial radial distribution functions at room temperature and concentrations of 20 wt%, 40 wt%, 60 wt%, 80 wt%, 90 wt% and 95 wt% (x = 0.045, 0.111, 0.220, 0.429, 0.628 and 0.781) are also displayed in Fig. 6. At dilutions of 20 wt%, $g_{OI\text{-}OW}(r)$ shows four peaks located at 0.28, 0.50, 0.62 and 0.89 nm, and three minima at 0.36, 0.55 and 0.77 nm. Moreover, $g_{OI\text{-}HW}(r)$ exhibits four maxima located at 0.18, 0.34, 0.40 and 0.55 nm, and three minima at 0.26, 0.36 and 0.46 nm. Similar results have recently been reported by Canales and Guàrdia [27] in their MD simulation study of sulfuric acid aqueous solutions. Note how the height of the peaks of both radial distribution functions increases when the concentration rises, being the effect more notorious at very large concentrations. The partial structure factors $S_{OI\text{-}OW}(k)$ and $S_{OI\text{-}HW}(k)$ have been also plotted in Fig. S1 of the supplementary material.

3.4.3. MSA(acceptor)-water radial distribution functions

The $g_{OA\text{-}OW}(r)$ and $g_{OA\text{-}HW}(r)$ partial radial distribution functions at room temperature and concentrations of 20 wt%, 40 wt%, 60 wt %, 80 wt%%, 90 wt% and 95 wt% (x = 0.045, 0.111, 0.220, 0.429, 0.628 and 0.781) are also displayed in Fig. 6. At dilutions of 20 wt%, $g_{OA\text{-}OW}(r)$ shows two peaks located at 0.31 and 0.55 nm, and two minima at 0.40 and 0.66 nm. Moreover, $g_{OA\text{-}HW}(r)$ exhibits five maxima located at 0.19, 0.34, 0.42, 0.60 and 0.90 nm, and four minima at 0.24, 0.36, 0.46 and 0.72 nm. Some of these peaks are very similar to those of the mesylate-water partial radial distribution functions $g_{OI\text{-}OW}(r)$ and $g_{OI\text{-}HW}(r)$. Also, note how the height of the peaks of both radial distribution functions increases when the concentration rises, being more notorious at very large concentrations. The partial structure factors $S_{OA\text{-}OW}(k)$ and $S_{OA\text{-}HW}(k)$ have been also plotted in Fig. S1 of the supplementary material.

3.4.4. Water-hydronium radial distribution functions

The $g_{OW\text{-}O3}(r)$ and $g_{OW\text{-}H3}(r)$ partial radial distribution functions at room temperature and concentrations of 20 wt%, 40 wt%, 60 wt%, 80 wt% %, 90 wt% and 95 wt% (x = 0.045, 0.111, 0.220, 0.429, 0.628 and 0.781) are plotted in Fig. 7. At dilutions of 20 wt %, $g_{OW\text{-}H3}(r)$ shows four maxima located at 0.165, 0.30, 0.40 and 0.54 nm, and three minima at 0.22, 0.345 and 0.47 nm. Moreover, $g_{OW\text{-}O3}(r)$ exhibits three peaks placed at 0.26 and 0.475 and 0.69 nm, and two minima at 0.365 and 0.56 nm. These results are very similar to those recently published by Canales and Guàr-

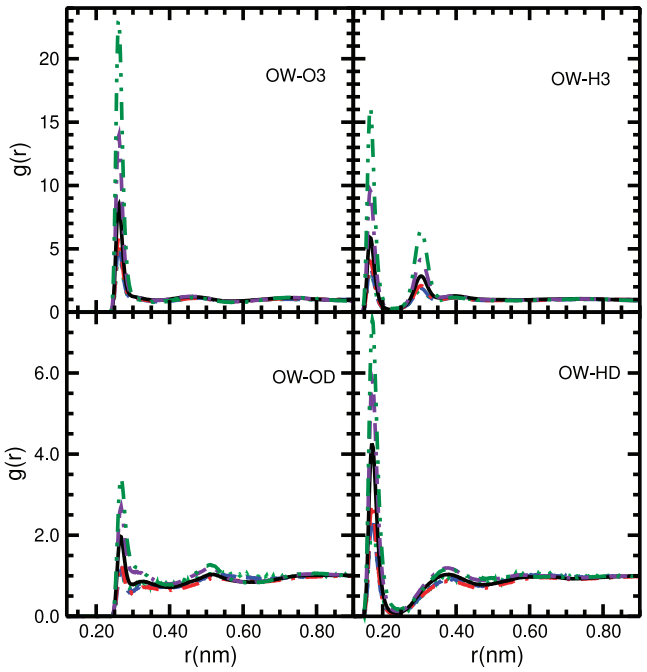

Fig. 7. Water-hydronium and water-MSA(donor) oxygen–oxygen and oxygen-hydrogen radial distribution functions at different concentrations: dotted line (green) 20 wt% (x = 0.045), dashed line (blue) 40 wt% (x = 0.111), dotted-dashed line (red) 60 wt% (x = 0.220), full line (black) 80 wt% (x = 0.429), dash-dash-dotted line (indigo) 90 wt% (x = 0.628) and dot-dot-dashed line (dark green) 95 wt% (x = 0.781). (For interpretation of the references to colour in this figure legend, the reader is referred to the web version of this article.)

dia [27] in their MD simulation study of sulfuric acid aqueous solutions. Note that the intensity of the main $g_{OW\text{-}O3}(r)$ and $g_{OW\text{-}H3}(r)$ peaks increases when the acid concentration rises. The partial structure factors $S_{OW\text{-}O3}(k)$ and $S_{OW\text{-}H3}(k)$ have been also plotted in Fig. S2 of the supplementary material.

3.4.5. Water-MSA(donor) radial distribution functions

The $g_{OW\text{-}OD}(r)$ and $g_{OW\text{-}HD}(r)$ partial radial distribution functions at room temperature and concentrations of 20 wt%, 40 wt%, 60 wt %, 80 wt%, 90 wt% and 95 wt% (x = 0.045, 0.111, 0.220, 0.429, 0.628 and 0.781) are also displayed in Fig. 7. At acid concentrations of 20 wt%, $g_{OW\text{-}OD}(r)$ shows three peaks located at 0.27, 0.34 and 0.52 nm, and three minima at 0.29, 0.4 and 0.65 nm. Moreover, $g_{OW\text{-}HD}(r)$ exhibits three maxima located at 0.17, 0.39 and 0.64 nm, and two minima at 0.23 and 0.48 nm. Also, note how the height of the first $g_{OW\text{-}OD}(r)$ and $g_{OW\text{-}HD}(r)$ peaks increase when the acid concentration rises. To a lesser extent, a similar slope behavior, to that previously reported for $g_{OW\text{-}OW}(r)$, has also been observed for $g_{OW\text{-}OD}(r)$ at high concentrations, which also indicates the vanishing of the second hydration shell around the oxygen atom of the MSA molecules hydroxyl group. Finally, the partial structure factors $S_{OW\text{-}OD}(k)$ and $S_{OW\text{-}HD}(k)$ have been also plotted in Fig. S2 of the supplementary material.

3.5. Mean number of hydrogen bonds

The mean number $<n_{HB}>$ of water molecules hydrogen bonded to every water molecule, in terms of the acid concentration, is plotted in Fig. 8 and gathered in Table S5 of the supplementary material. $<n_{HB}>$ decreases linearly when the concentration rises. This behavior has also been reported by Canales and Guàrdia [27] for dilute and moderate aqueous sulfuric acid solutions, and by Hartkamp and Coasne [66] for some aqueous electrolyte solutions. To

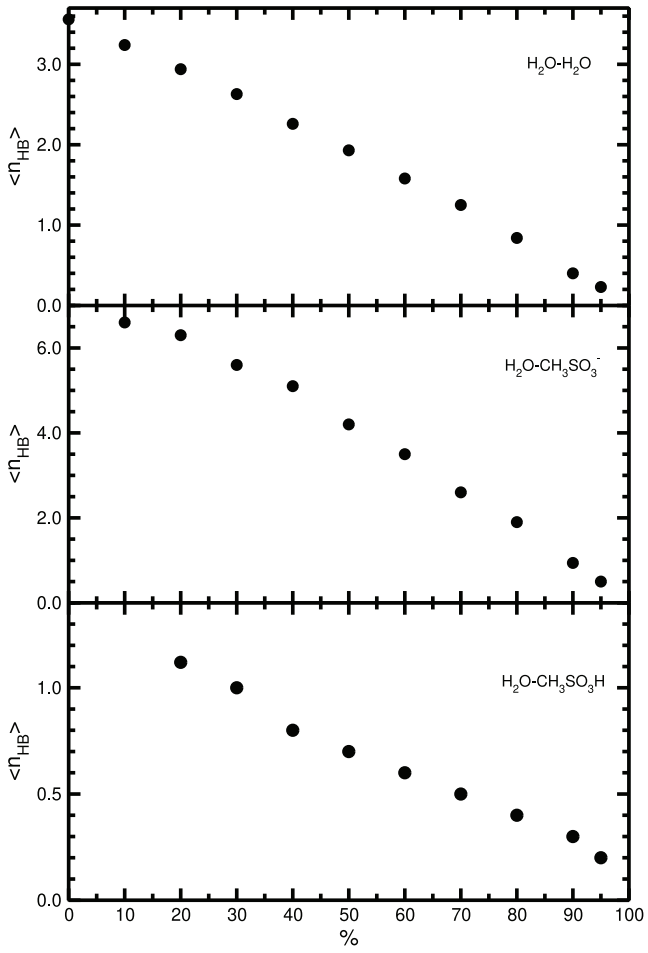

Fig. 8. Mean number of HB for different concentrations. Water-water (up), water-mesylate (middle), and water-MSA-acceptor (down).

shed more light on this tendency we have also computed the percentages f_n of water molecules bonded to other "n" water molecules. The results have been plotted in Fig. 9 and also collected in Table S5 of the supplementary material. The characteristic HB network of pure water is quickly broken because water molecules tend to bond mainly with the ions, and to a lesser extent with the MSA molecules, as the concentration increases. Then, at low dilutions (10–20 wt%, x = 0.020–0.045) there is a reduction of f_4 and f_5 and an increase of f_2 and f_3. At moderate concentrations (up to 50 wt%, x = 0.158) there is also a reduction of f_3 and an increase of f_1 and f_0. Finally, at larger concentrations, each water molecule tends to bond at most with only one water molecule.

The average number $<n_{HB}>$ of water molecules bonded to each mesylate anion is also plotted in Fig. 8 and gathered in Table S6 of the supplementary material. $<n_{HB}>$ also decreases when the concentration rises. Canales and Guàrdia [27] observed similar behavior for dilute and moderate aqueous sulfuric acid solutions. We have also analyzed the percentages f_n of mesylate anions bonded to "n" water molecules. These results have been displayed in Fig. 9 and collected in Table S6 of the supplementary material. At low concentrations (10 wt%, x = 0.020), each mesylate is hydrogen bonded to 6 or 7 water molecules. This number quickly decreases when the concentration increases. For instance, each mesylate anion is respectively bonded to 4 and 2 water molecules at 50 wt % and 80 wt% (x = 0.158 and 0.429) acid solutions.

Now we turn to the study of the HB between water and MSA(acceptor) molecules. The average number $<n_{HB}>$ of water molecules

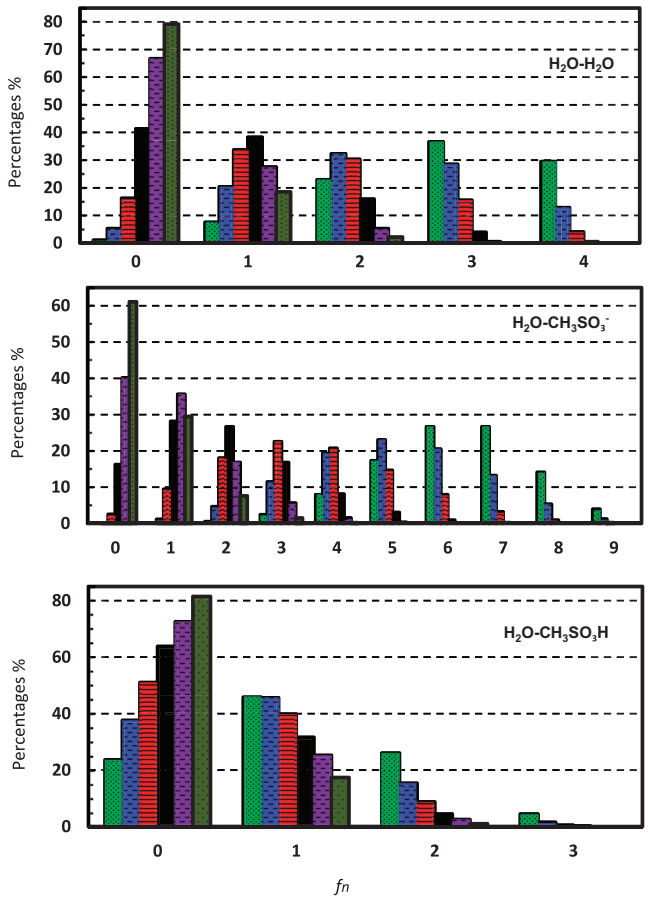

Fig. 9. Histograms with the percentages f_n of water molecules, mesylate ions and MSA(acceptor) molecules bonded with "n" water molecules for different concentrations: green and dotted 20 wt% (x = 0.045), blue and dashed 40 wt% (x = 0.111), red and full line 60 wt% (x = 0.220), black 80 wt% (x = 0.429), indigo and dashed 90 wt% (x = 0.628), and dark green and dotted 95 wt% (x = 0.781). (For interpretation of the references to colour in this figure legend, the reader is referred to the web version of this article.)

hydrogen bonded to each MSA molecule, for aqueous solutions of up 20 wt% (x = 0.045), is plotted in Fig. 8 and gathered in Table S7 of the supplementary material. Moreover, we have also analyzed the percentages f_n of MSA molecules bonded to "n" water molecules. The results have been shown in Fig. 9 and collected in Table S7 of the supplementary material. At moderate concentrations (up to 40 wt%, x = 0.111) each acid molecule is bonded to only one water molecule, and this ratio decreases when the acid concentration rises.

Some years ago, Botti *et al.* [67] explored the solvation shell around one hydronium ion, using a combination of neutron diffraction experiments and Monte Carlo simulation techniques. They concluded that each H+ ion is captured by a water molecule giving rise to a hydronium ion H_3O^+, which is hydrogen bonded to the other three water molecules, belonging to its first coordination shell. This finding is in good agreement with our results of the average number $<n_{HB}>$ of water molecules hydrogen bonded to each hydronium ion, which is displayed in Fig. 10 and gathered in Table S8 of the supplementary material. They also agree with the results of the percentages f_n of hydronium ions bonded to "n" water molecules, which are depicted in Fig. 11 and collected in Table S8 of the supplementary material. Then, at dilute (10 wt%, x = 0.020) solutions the average number $<n_{HB}>$ is 2.7. However, this number dramatically decreases when the acid concentration rises.

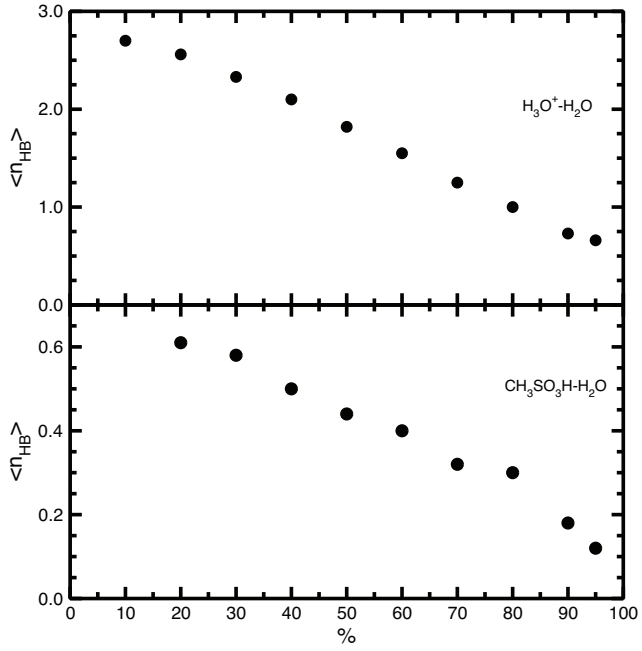

Fig. 10. Mean number of HB for different concentrations. Hydronium-water (up) and MSA(donor)-water (down).

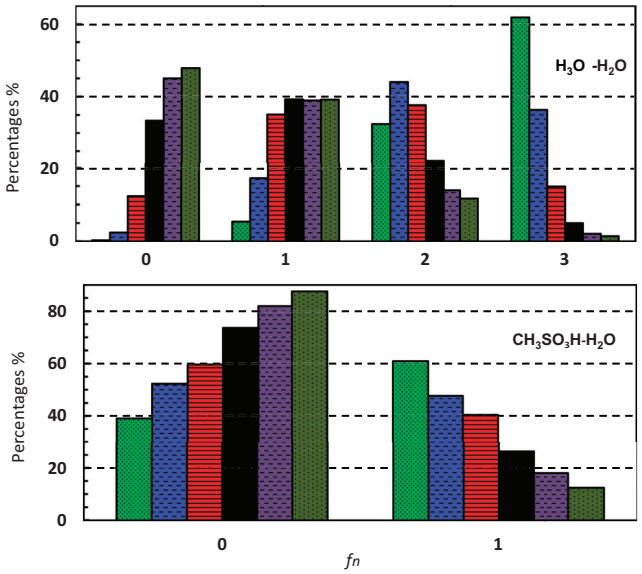

Fig. 11. Histograms with the percentages f_n of hydronium ions and MSA(donor) molecules bonded with "n" water molecules for different concentrations: green and dotted 20 wt% (x = 0.045), blue and dashed 40 wt% (x = 0.111), red and full line 60 wt% (x = 0.220), black 80 wt% (x = 0.429), indigo and dashed 90 wt% (x = 0.628), and dark green and dotted 95 wt% (x = 0.781). (For interpretation of the references to colour in this figure legend, the reader is referred to the web version of this article.)

Finally, we turn to the study of the HB between water and MSA (donor) molecules. The average number $<n_{HB}>$ of water molecules hydrogen bonded to each MSA molecule is plotted in Fig. 10 and gathered in Table S9 of the supplementary material. Moreover, we have also analyzed the percentages f_n of MSA molecules bonded to "n" water molecules. The results have been displayed in Fig. 11 and collected in Table S9 of the supplementary material. Note that at 20 wt% and 40 wt% (x = 0.045 and 0.111) the mean number of water molecules hydrogen bonded to one MSA molecule are

respectively 0.6 and 0.5. This number quickly decreases at higher concentrations.

3.6. Hydrogen bond lifetimes

Some years ago, Chandler and Luzar [68,69] developed a well-established methodology to compute HB lifetimes. Particularly, they introduced two different lifetimes, named non-interrupted and interrupted. The non-interrupted, continuous or fast lifetime τ_{CHB} is set up assuming that a given HB remains always unbroken. It is calculated from the time integral of the probability $P(t)$ function that two molecules, that are initially bonded, remain always bonded. $P(t)$ is computed by constructing a histogram of the HB lifetimes for all configurations.

The interrupted or slow lifetime is construed by postulating that a given HB can break and re-form. The lifetime is calculated by introducing the probability function $c(t)$ that a pair of molecules is bonded at time t, provided that the same pair was initially bonded. Therefore, $c(t)$ is determined according to the following relation:

$$c(t) = < h(t)h(0) > / < h(0)^2 >$$

$h(t)$ is a binary function, which is defined as follows: $h(t) = 1$ if a given pair of molecules "i,j" are bonded at time t, and $h(t) = 0$ otherwise. Initially, $c(t)$ decays exponentially and later it continues diminishing according to a long tail, which can be modeled by a power law relationship. At a first glance, the lifetime could be obtained by the simple time integration of $c(t)$. Nevertheless, the self-diffusion of the solvent molecules induces smaller HB relaxation values [70]. This issue can be circumvented by employing an auxiliary correlation function $n(t)$, which is formulated as [69]:

$$n(t) = < h(0)[1 - h(t)]H(t) > / < h(0) >$$

$H(t)$ is a new binary function that is detailed as follows: $H(t) = 1$ if the distance between the oxygen atoms of the pair of molecules "i,j" that are hydrogen bonded is closer than the first minimum of the $g_{O\text{-}O}(r)$ radial distribution function at time t, and $H(t) = 0$ otherwise. Therefore, the HB dynamics can be analyzed by employing the reactive flux correlation function $k(t) = -dc(t)/dt$, which Luzar and Chandler [69] related to the $n(t)$ and $c(t)$ functions by the following equation:

$$k(t) = kc(t) - k'n(t)$$

k and k' are the rate parameters, which respectively correspond to the HB break and re-formation processes. At intermediate times $k(t)$ decreases following an exponential law, which is normally employed to calculate the interrupted or slow lifetime τ_{IHB}.

The continuous or non-interrupted lifetimes at room temperature in the entire acid concentration range have been plotted in Fig. 12 and collected in Table S10 of the supplementary material. The HB lifetimes between water molecules and mesylate anions, and those between MSA(acceptor) and water molecules are approximately half the ones between: 1) water molecules, 2) water molecules and hydronium cations, and 3) water and MSA(donor) molecules. This finding is in qualitatively good agreement with that previously noticed for sulfuric acid solutions by Canales and Guàrdia [27]. These authors stated that the water molecules bonded to the anions were more labile than those bonded to other water molecules or hydronium cations. Finally, it is important to note that, at large concentrations, the lability of the water molecules, bonded to other water molecules, increases, and that of the water molecules, bonded to hydronium ions, decreases.

The interrupted water-water τ_{IHB} HB lifetimes are displayed in Fig. 13 and also gathered in Table S11 of the supplementary material. At low concentrations, the values are very close to those pre-

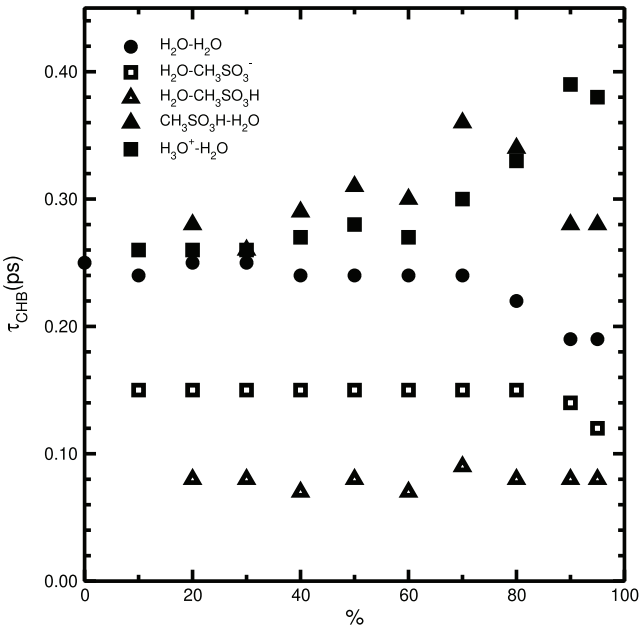

Fig. 12. Continuous HB lifetimes at several concentrations. Water-water (solid circles), water-mesylate (open squares), water-MSA(acceptor), MSA(donor)-water (solid triangles), and hydronium-water (solid squares).

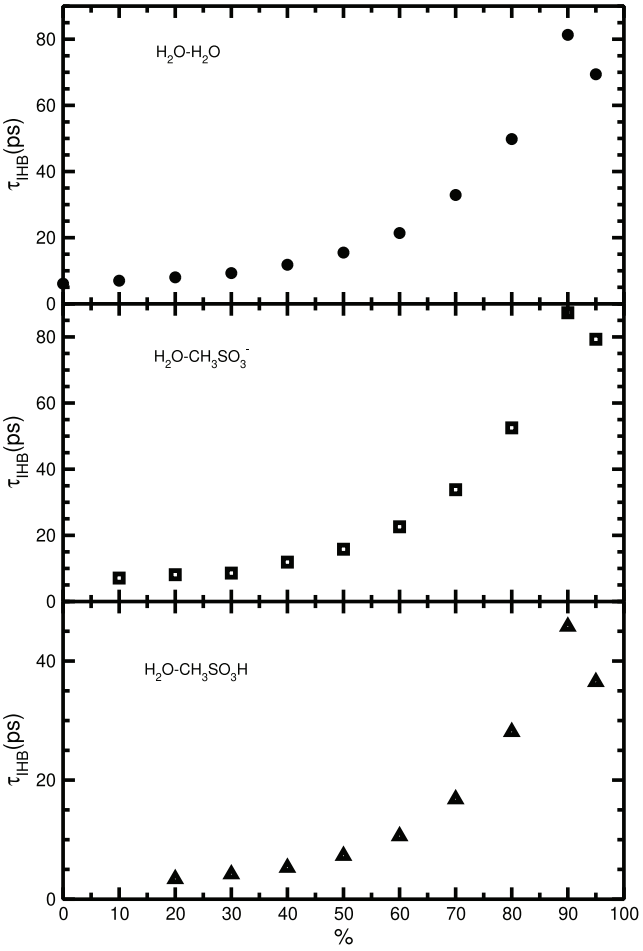

Fig. 13. Interrupted HB lifetimes at several concentrations. Water-water (up), water-mesylate (middle), and water-MSA(acceptor) (down).

viously reported by Starr *et al.* [71] (τ_{IHB} = 5.18 ps) in their classical MD study of pure water using the SPCE model, and those of Guàrdia *et al.* [72] employing the Car-Parrinello methodology (τ_{IHB} = 4.90 ps). The values increase as the acid concentration rises showing a unimodal dependence, with a maximum located at 90 wt% (x = 0.628).

Now we turn to the analysis of the HB between water molecules and mesylate ions, and also to those between water and MSA(acceptor) molecules. In the first case, the τ_{IHB} lifetimes are plotted in Fig. 13 and gathered in Table S11 of the supplementary material. The values are very similar to those for water-water, and they also display a maximum at 90 wt% (x = 0.628). The interrupted τ_{IHB} lifetimes between water and MSA molecules are also shown in Fig. 13 and collected in Table S11 of the supplementary material. Now, the values are approximately half the ones of the water-water and the mesylate-water cases. This illustrates that the HB between water molecules, and water molecules and mesylate ions are stronger than those between MSA and water molecules. This result can also be explained by analyzing the differences between the intensities of the first peaks of the radial distribution functions $g_{OW\text{-}OW}(r)$, $g_{OI\text{-}OW}(r)$, $g_{OA\text{-}OW}(r)$, $g_{OW\text{-}HW}(r)$, $g_{OI\text{-}HW}(r)$ and $g_{OA\text{-}HW}(r)$, plotted in Fig. 6. At last, note how the interrupted lifetimes τ_{IHB} shown in Fig. 13 also exhibit a maximum at 90 wt% (x = 0.628).

Now we focus on the HB between water molecules and hydronium ions, and water and MSA(donor) molecules. In the first case, the τ_{IHB} lifetimes have been plotted in Fig. 14 and gathered in Table S11 of the supplementary material. Note that the values are larger than those of the HB between water molecules, in the entire acid concentration range. This behavior reveals that the HB between hydronium ions and water molecules are stronger than those between water molecules. This finding can also be explained by analyzing the differences in the intensities of the first $g_{OW\text{-}OW}(r)$, $g_{OW\text{-}O3}(r)$, $g_{OW\text{-}HW}(r)$ and $g_{OW\text{-}H3}(r)$ peaks, displayed in Figs. 6 and 7. Note that in this case, the lifetimes do not exhibit a unimodal concentration dependence. Finally, the τ_{IHB} lifetimes between MSA and water molecules are also shown in Fig. 14 and gathered in Table S11 of the supplementary material. Note that the values are smaller than those of the HB between water molecules and hydronium ions, and they also exhibit a unimodal concentration dependence, with a maximum at 90 wt% (x = 0.628).

The unimodal concentration dependence of the interrupted lifetimes, with a maximum at 90 wt%, is very similar to that previously observed for the shear viscosity in section III-A. Dougan *et al.* [73] reported a qualitatively similar behavior for methanol-water binary mixtures. Indeed, these authors, who conducted a series of neutron diffraction experiments and MD simulations, noticed that at the methanol mole fraction of 0.27, the viscosity exhibits its maximum, and the hydrogen bonding interactions induce a bipercolating (methanol/water) network structure at this concentration value. This finding was corroborated by the MD simulations of Bakó *et al.* [74] and Zhang *et al.* [75], who, respectively, analyzed the topology of the HB networks, and studied the influence of the temperature and concentration on the HB structure and the diffusion coefficients. We propose a different interpretation for aqueous MSA solutions. Indeed, as it is well-known, pure water shows a HB three-dimensional tetrahedral network [25], and conforming to Canales *et al.* [12,13], pure MSA exhibits a linear HB structure that resembles the one of methanol. According to Table 3, the acid dissociates almost completely at low and moderate concentrations (α > 0.9 at concentrations lower than 45 wt%, x = 0.135). Therefore, the characteristic water HB network quickly vanishes as the concentration rises, because the water molecules tend to bond to the mesylate and hydronium ions. Moreover, conforming to Figs. 8 and 10, the mean number of water molecules bonded to each species decreases as the concentration rises. At 90 wt% (x = 0.628) the number of MSA molecules is large enough (α = 0.246) that a HB structure, similar to that of pure MSA, appears. Therefore, the maximum of the viscosity, the minima of the diffusion coefficients and the maxima of the interrupted lifetimes at 90 wt%, could be related to the appearance of an incipient MSA HB structure, but not to a bipercolating HB network, as in the case of the methanol-water binary mixtures, where no dissociation effects are present. This interpretation deserves more detailed analysis, and future work will be done in that direction.

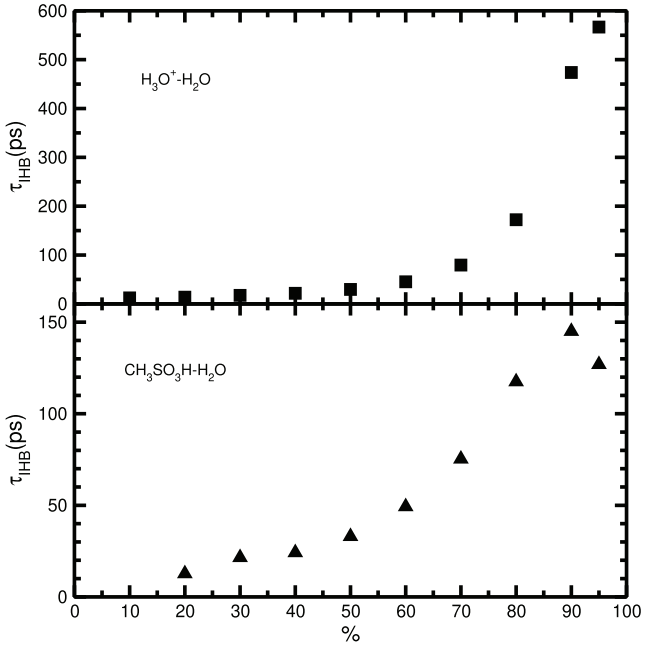

Fig. 14. Interrupted HB lifetimes at several concentrations. Hydronium-water (up) and MSA(donor)-water (down).

4. Conclusions

MD simulations of aqueous MSA solutions at room temperature in the entire acid concentration range have been carried out. The dissociation of the acid has been considered according to the available experimental data. The simulated systems are constituted by the following molecular species: water molecules, hydronium cations, methanesulfonate anions (mesylate ions), and MSA molecules. A reliable force field has been employed, which provides a sound agreement between the experimental and the simulated data for the density at all concentrations. MD simulations have also been carried out to compute the shear viscosity coefficients and the radial distribution functions, which involve water molecules. Although, to our knowledge, there are no experimental data in the literature on the viscosities of MSA aqueous solutions in terms of concentration, we believe that our results are quite reasonable because, on one hand, they are similar to those obtained recently for moderate aqueous sulfuric acid solutions and, on the other hand, because our findings for pure water and MSA are very close to the experimental values. The viscosity shows a concentration unimodal dependence, with the maximum located at 90 wt% (x = 0.628). The changes in the water oxygen–oxygen and the oxygen-hydrogen radial distribution functions are particularly noticeable at very large concentrations. Additionally, we have also calculated the diffusion coefficient of the constituent species, which also show the same concentration unimodal dependence, but in this case with minima, located at 90 wt%. Moreover, the

water molecules diffuse more than the other constituent species in the whole range of concentrations.

An analysis of the hydrogen bonds involving water molecules has also been conducted. To this end, we have computed the following properties: the mean number $<n_{HB}>$ of HB, the percentages f_n of molecular species (water, mesylate anion, MSA and hydronium cation) bonded with "n" water molecules, the continuous τ_{CHB} and the interrupted τ_{IHB} lifetimes. The results of the continuous lifetimes τ_{CHB} illustrate that the water molecules bonded to the mesylate anions and those bonded to MSA(acceptor) molecules are more labile than those bonded to other water molecules, to the hydronium ions or MSA(donor) molecules. Moreover, at low and moderate dilutions the continuous τ_{CHB} lifetimes do not significantly change when the concentration increases. However, at large concentrations, the lability of the water molecules bonded to other water molecules increases, and that of the water molecules bonded to the hydronium cations decreases. Moreover, the interrupted HB lifetimes increase when the concentration rises, verifying the following relation in the entire concentration range: $\tau_{IHB}(H_2O\text{--}CH_3SO_3H) < \tau_{IHB}(H_2O\text{-}H_2O) = \tau_{IHB}(H_2O\text{-}CH_3SO_3^-) < \tau_{IHB}(CH_3SO_3H\text{-}H_2O) < \tau_{IHB}(H_3O^+\text{-}H_2O)$. Note that the interrupted lifetimes of the water molecules bonded to the MSA(donor) molecules are larger than the MSA(acceptor) ones. These results, allow us to suggest the following description of the water molecules HB in aqueous MSA solutions, in terms of the concentration: At low dilutions, water exhibits its characteristic tetrahedral structure. When the acid concentration increases, the water molecules tend to bond to the ions or the MSA molecules. Then, the percentages of water molecules hydrogen bonded to the other four water molecules f_4 decrease. At the same time, the interrupted τ_{IHB} lifetimes and the percentages of water molecules bonded to one or two water molecules f_1 and f_2 increase. Finally, the mean number and the percentages f_n of ions or molecules hydrogen bonded with a large "n" number of water molecules decreases and the interrupted HB lifetimes increase, being more notorious when the oxygen atoms of the water molecules are HB acceptors. At 90 wt% (x = 0.628) the interrupted HB lifetimes exhibit a maximum, that could be related to the appearance of an incipient MSA HB network.

Data availability

Data will be made available on request.

Declaration of Competing Interest

The authors declare that they have no known competing financial interests or personal relationships that could have appeared to influence the work reported in this paper.

Acknowledgements

Financial support from the Ministerio de Ciencia e Innovación of Spain, Grants PGC2018-099277-B-C21(MCIU/AEI/ERDF) and PID2021-124297NB-C32 (MCIN/AEI/10.13039 /501100011033/ ERDF) is gratefully acknowledged.

Appendix A. Supplementary data

Supplementary data to this article can be found online at https://doi.org/10.1016/j.molliq.2023.121518.

References

[1] S. Patai, Z. Rappoport, The Chemistry of Sulphonic Acids, Esters and Their Derivatives, John Wiley & Sons, New York, 1991.
[2] F.C. Walsh, C. Ponce de León, Surf. Coat. Technol. 259 (2014) 676.
[3] M.D. Gernon, M. Wu, T. Buzsta, P. Janney, Green Chem. 1 (1999) 127.
[4] T.A. Skotheim, R.L. Elsenbaumer, J.R. Reynolds, Handbook of Conducting Polymers, Marcel Dekker, New York, 1998.
[5] T. Palden, B. Onghena, M. Regadío, K. Binnemans, Green Chem 21 (2019) 5394.
[6] O. Boucher, Atmospheric Aerosols: Properties and Climate Impacts, Springer, Netherlands, 2015.
[7] R.J. Charlson, J.E. Lovelock, M.O. Andreae, S.G. Warren, Nature 326 (1987) 655.
[8] M.L. Dawson, M.E. Varner, V. Perraud, M.J. Ezell, R.B. Gerber, B.J. Finlayson-Pitts, PNAS 109 (2012) 18719.
[9] S.C. Baker, D.P. Kelly, J.C. Murrell, Nature 350 (1991) 627.
[10] T.T. Teng, F. Lenzi, J. Chem. Eng. Data 20 (1975) 432.
[11] C.E. Lund Myhre, B. D'Anna, F.M. Nicolaisen, C.J. Nielsen, Appl. Opt. 43 (2004) 2500.
[12] M. Canales, C. Alemán, J. Phys. Chem. B 118 (2014) 3423.
[13] M. Canales, E. Guàrdia, J. Mol. Liq. 224 (2016) 1064.
[14] A. Krishtal, P. Senet, C. Van Alsenoy, J. Chem. Theory Comput. 4 (2008) 2122.
[15] L. Wang, J. Phys. Chem. A 111 (2007) 3642.
[16] S. Li, W. Qian, F.-M. Tao, Chem. Phys. Lett 438 (2007) 190.
[17] S.M. Kreidenweis, J.H. Seinfeld, Atmos. Environ 22 (1988) 283.
[18] K.N. Bascombe, R.P. Bell, J. Chem. Soc. 1096–1104 (1959).
[19] A.K. Covington, T.H. Lilley, Trans. Faraday Soc. 63 (1967) 1749.
[20] A.K. Covington, R. Thompson, J. Solut. Chem. 3 (1974) 603.
[21] J.H.R. Clarke, I.A. Woodward, Trans. Faraday Soc. 62 (1966) 2226.
[22] G.A. Jeffrey, An Introduction to Hydrogen Bonding, Oxford University Press, New York, 1997.
[23] S.J. Grabowski (Ed.), Hydrogen Bonding-New Insights, Springer, Dordrecht, 2006.
[24] B.M. Ladanyi, M.S. Skaf, Annu. Rev. Phys. Chem. 44 (1993) 335.
[25] Y. Marechal, The Hydrogen Bond and the Water Molecule: The Physics and Chemistry of Water, Aqueous and Bio-Media (Elsevier, Amsterdam, 2007.
[26] M. Canales, E. Guàrdia, J. Mol. Liq. 293 (2019) 111463.
[27] M. Canales, E. Guàrdia, J. Mol. Liq. 347 (2022) 118351.
[28] H. Arstila, K. Laasonen, A. Laaksonen, J. Chem. Phys. 108 (1998) 1031.
[29] H.J.C. Berendsen, J.R. Grigera, T.P. Straatsma, J. Phys. Chem. 91 (1987) 6269.
[30] C. Vega, J.L.F. Abascal, Phys. Chem. Chem. Phys 13 (2011) 19663.
[31] S.P.K. Pathirannahalage, N. Meftahi, A. Elbourne, A.C.G. Weiss, C.F. McConville, A. Padua, D.A. Winkler, M.C. Gomes, T.L. Greaves, T.C. Le, Q.A. Besford, A.J. Christofferson, J. Chem. Inf. Model. 61 (2021) 4521.
[32] J.L.F. Abascal, C. Vega, J. Chem. Phys 123 (2005).
[33] A. Baranyai, P.T. Kiss, J. Chem. Phys. 133 (2010) 144109.
[34] A. Baranyai, P.T. Kiss, J. Chem. Phys. 135 (2011) 234110.
[35] P.T. Kiss, M. Darvas, A. Baranyai, P. Jedlovszky, J. Chem. Phys 136 (2012).
[36] P.T. Kiss, A. Baranyai, J. Chem. Phys. 137 (2012).
[37] P.T. Kiss, A. Baranyai, J. Chem. Phys. 138 (2013).
[38] Z. Steinczinger, P. Jóvári, L. Pusztai, J. Mol. Liq. 228 (2017) 19.
[39] I. Kusaka, Z.G. Wang, J.H. Seinfeld, J. Chem. Phys. 108 (1998) 6829.
[40] O. Teleman, B. Jönsson, S. Engström, Mol. Phys. 60 (1987) 193.
[41] J.P. Ryckaert, A. Bellemans, Chem. Phys. Lett. 30 (1975) 123.
[42] I.V. Leontyev, A.A. Stuchebrukhov, J. Chem. Phys. 130 (2009).
[43] I.V. Leontyev, A.A. Stuchebrukhov, J. Chem. Theory Comput. 6 (2010) 1498.
[44] I.V. Leontyev, A.A. Stuchebrukhov, Phys. Chem. Chem. Phys. 13 (2011) 2613.
[45] I.V. Leontyev, A.A. Stuchebrukhov, J. Chem. Theory Comput. 8 (2012) 3207.
[46] I.V. Leontyev, A.A. Stuchebrukhov, J. Chem. Phys. 141 (2014).
[47] Z.R. Kann, J.L. Skinner, J. Chem. Phys. 141 (2014).
[48] I.M. Zeron, J.L.F. Abascal, C. Vega, J. Chem. Phys. 151 (2019).
[49] B. Hess, C. Kutzner, D. van der Spoel, J. Chem. Theory Comput. 4 (2008) 435.
[50] J.P. Ryckaert, G. Cicotti, H.J.C. Berendsen, J. Comput. Phys. 23 (1977) 327.
[51] H.J.C. Berendsen, J.P.M. Postma, W.F. van Gunsteren, A. DiNola, J.R. Haak, J. Chem. Phys. 81 (1984) 3684.
[52] M.P. Allen, D.J. Tildesley, Computer Simulation of Liquids, Oxford University Press, New York, 1987.
[53] T. Darden, D. York, L. Pedersen, J. Chem. Phys. 98 (1993) 10089.
[54] A.R. Leach, Molecular Modelling: Principles and Applications, Pearson, Harlow, 2001.
[55] B. Hess, J. Chem. Phys. 116 (2002) 209.
[56] M.A. González, J.L.F. Abascal, J. Chem. Phys. 132 (2010).
[57] D.B. Roitman, J. McAlister, F.L. Oaks, J. Chem. Eng. Data 39 (1994) 56.
[58] F.H. Rhodes, C.B. Barbour, Ind. Eng. Chem. 15 (1923) 850.
[59] J.D. Isdale, A.J. Easteal, L.A. Woolf, Int. J. Thermophys. 6 (1985) 439.
[60] R.L. Kay, T.L. Broadwater, J. Solution Chem. 5 (1976) 57.
[61] G. Guevara-Carrion, J. Vrabec, H. Hasse, J. Chem. Phys. 134 (2011).
[62] D. Bertolini, M. Cassettari, M. Ferrario, P. Grigolini, G. Salvetti, Adv. Chem. Phys. 62 (1985) 277.
[63] J. Martí, J. Chem. Phys. 110 (1999) 6876.
[64] P. Mark, L. Nilsson, J. Phys. Chem. A 105 (2001) 9954.
[65] P. Gallo, D. Corradini, M. Rovere, J. Mol. Liq. 189 (2014) 52.
[66] R. Hartkamp, B. Coasne, J. Chem. Phys. 141 (2014).
[67] A. Botti, F. Bruni, S. Imberti, M.A. Ricci, A.K. Soper, J. Mol. Liq. 117 (2005) 77.
[68] A. Luzar, D. Chandler, Nature 379 (1996) 55.
[69] A. Luzar, J. Chem. Phys. 113 (2000) 10663.

[70] H.S. Lee, M.E. Tuckerman, J. Chem. Phys. 126 (2007).
[71] F.W. Starr, J.K. Nielsen, H.E. Stanley, Phys. Rev. E 62 (2000) 579.
[72] E. Guàrdia, I. Skarmoutsos, M. Masia, J. Phys. Chem. B 119 (2015) 8926.
[73] L. Dougan, S.P. Bates, R. Hargreaves, J.P. Fox, J. Crain, J.L. Finney, V. Réat, A.K. Soper, J. Chem. Phys. 121 (2004) 6456.
[74] I. Bakó, T. Megyes, S. Bálint, T. Grósz, V. Chihaia, Phys. Chem. Chem. Phys. 10 (2008) 5004.
[75] N. Zhang, Z. Shen, C. Chen, G. He, C. Hao, J. Mol. Liq. 203 (2015) 90.